Environ Monit Assess (2024) 196:1105
https://doi.org/10.1007/s10661-024-13224-7

RESEARCH

Evapotranspiration measurements in pasture, crops, and native Brazilian Cerrado based on UAV-borne multispectral sensor

Gabriella Santos Arruda de Lima · Manuel Eduardo Ferreira · Jepherson Correia Sales · Joelson de Souza Passos · Selma Regina Maggiotto · Beata Emoke Madari · Márcia Thaís de Melo Carvalho · Pedro Luiz Oliveira de Almeida Machado

Received: 28 May 2024 / Accepted: 8 October 2024

Abstract In Brazil, agriculture consumes most of the available freshwater, especially in the Cerrado biome, where the rain cycle is marked by long periods of drought. This study, conducted at the Brazilian Agricultural Research Corporation (Embrapa) Research Corporation unit in Santo Antônio de Goiás, Goiás, Brazil, estimated evapotranspiration (ET) in different crops and soil cover. Using multispectral unmanned aerial vehicle (UAV) images, Sentinel satellite data, weather station information, and towers employing the eddy covariance method, we applied the "Simple Algorithm for Evapotranspiration Retrieving" (SAFER) to calculate ET in common bean, pasture, and semideciduous seasonal forest areas. The results showed a good agreement between UAV and satellite data, with $R^2 = 0.84$, also validated with flow towers by the eddy covariance method. UAV-based ET was observed to correspond well to tower (EC) during full vegetative development of beans but is underestimated at the beginning of planting and in the final periods of plant senescence, due to the influence of soil or straw cover. These findings contribute to a better understanding of water dynamics in the system and to enhancing sustainable agricultural practices. This method, adapted for multispectral aerial imaging, can be applied flexibly and on-demand, in different contexts and ground cover. The study highlights the importance of integrated agricultural practices for better management of water resources and preservation of the Cerrado in balance with cultivation areas.

Keywords Evapotranspiration · UAV · Cerrado · Sustainable practices · Water resources

G. S. A. de Lima (✉) · M. E. Ferreira · J. de Souza Passos
Image Processing and GIS Laboratory (LAPIG), Federal University of Goiás (UFG), Goiânia, GO, Brazil
e-mail: gabriella.arruda.lima@gmail.com

M. E. Ferreira
e-mail: manuel@ufg.br

J. de Souza Passos
e-mail: joelson3000@gmail.com

J. C. Sales
Department of Geography, Federal University of Rondonópolis, Rondonópolis, MT, Brazil
e-mail: jepherson.sales@ufr.edu.br

S. R. Maggiotto
Department of Agronomy, University of Brasília, AgrometeorologyBrasília, DF, Brazil
e-mail: srmaggio2@gmail.com

B. E. Madari · M. T. de Melo Carvalho · P. L. O. de Almeida Machado
Embrapa Arroz E Feijão, Santo Antônio de Goiás, GO, Brazil
e-mail: beata.madari@embrapa.br

M. T. de Melo Carvalho
e-mail: marcia.carvalho@embrapa.br

P. L. O. de Almeida Machado
e-mail: pedro.machado@embrapa.br

Published online: 25 October 2024

Introduction

Freshwater scarcity threatens food and water security in many parts of the world. In Brazil, it is estimated that of the total water expenditure for human activities, a percentage of 69% is destined to agriculture, a value very close to the world average (70%) (Christofidis, 2001). The Cerrado, the second largest biome in South America (originally occupying 2 million km^2 of Brazilian territory), plays a unique role in the continent's water dynamics, housing the springs of 12 of the country's main hydrographic regions (Ferreira, et al., 2022). Centrally located and quite extensive, this biome is responsible for up to 80% of energy production (MMA, 2014) and approximately 50% of grain and meat production in Brazil (Queiroz, 2009).

The Cerrado's water regime is marked by a rainy and a dry season, each lasting ~ 6 consecutive months (drought between May and September). Although temporary agricultural production is concentrated in the rainy season (with first crop plantations occurring in October), this climatic condition requires planning for the use of irrigation systems, especially in perennial or established crops in the dry months. Currently, about 50% of the native area of this biome is converted to anthropogenic activities, especially cultivated and native pastures (~ 34%) and agriculture (~ 14%), especially soybeans, corn, and sugarcane, in addition to mining and urban areas (MapBiomas, 2022; Sano et al., 2019; Strassburg et al., 2017). It is known, however, that changes in land use and land cover have a direct impact on ecosystem functions, notably influencing seasonal variability in mass and energy exchange processes (Ivo et al., 2020).

In turn, the improvement in the management of water resources requires the correct sizing of water present in the system through the understanding of the hydrological cycle (Guo et al., 2008). Evapotranspiration (ET) plays a crucial role in identifying these changes caused by human activities and climate change in agricultural and natural systems, which exhibit notable regional contrasts in the Midwest region of Brazil (da Silva et al., 2019; Dias et al., 2015). In a simplified way, ET can be understood as the transfer of water from the soil–plant system to the atmosphere, under any condition of humidity and vegetation cover. The determination of ET is the target of several studies, with different techniques and methodologies, which aim to get closer and closer to the field reality. ET is highly influenced by local climatic conditions, suffering variations with wind speed, solar radiation intensity, and air temperature (Teixeira & Lima Filho, 2004). Direct measurement methods, such as the use of lysimeters, monitoring towers, and soil water balance, provide reliable results. Eddy Covariance Flux measurement towers provide continuous, real-time measurements of energy flows in the atmosphere at a specific point, enabling a detailed understanding of the interactions between the Earth's surface and the atmosphere on fine time scales. However, they do not cover large areas, having little representation of field variability. An alternative of great use is indirect methods that employ remote image sensing techniques (satellites and UAV), as they have greater detail and variation of information in each pixel, making it a cheaper and reliable method (Hafeez et al., 2023).

In the estimation of ET, methods based on orbital remote sensing (i.e., by satellite images) are more used than those based on aerial images, lately provided by unmanned aerial platforms, known as drones or unmanned aerial vehicle (UAV). Thermal and multispectral cameras on board UAVs are relatively recent in the market, and therefore the expressive growth of research to estimate ET with such technology (Mokhtari et al., 2021; Nassar et al., 2020; Xia et al., 2016). Although these works address the topic in depth, there is still a knowledge gap regarding the application of UAV-based ET models, especially in Brazil, in biomes such as the Cerrado. Thus, studies that use satellite images from the Landsat and Sentinel series (Mokhtari et al., 2021; Safre et al., 2022), or MODIS (Silva Oliveira et al., 2018; Veloso et al., 2017), are still the vast majority, bringing satisfactory estimates of ET for larger areas. The use of sensors embedded in UAVs, on the other hand, offers ET maps on a cartographic scale of great detail, generated frequently and quickly, which is fundamental for agricultural management at the level of a field or agricultural parcel.

In this study, it is crucial to highlight the different scales of measurement used in the estimation of evapotranspiration (ET). Each method, whether UAV-based, satellite-derived, or eddy covariance (EC) tower measurements, operates at distinct spatial and temporal scales, serving different purposes. While UAV-based data provide high-resolution, detailed

ET maps at the field level, satellite images like those from Sentinel and Landsat offer broader, regional-scale insights. On the other hand, the eddy covariance method, though limited to point-based measurements, delivers continuous and precise energy flow data. These methods are comparable at specific points, yet they fulfill complementary roles in understanding ET across various scales, making this contextualization vital for interpreting the study's results.

Among the various models employed to estimate evapotranspiration (ET), the Simple Algorithm for Evapotranspiration Retrieving (SAFER) is notable for its simplified application. Unlike the Surface Energy Balance Algorithm for Land (SEBAL) model, which demonstrates a high sensitivity to the need to identify cold and warm reference pixels in temperature images, SAFER dispenses with this requirement. According to Teixeira et al. (2012), the identification of hot or dry pixel is complex in rainy seasons, since, in this period, natural vegetation may present latent heat flow rates (λE) even higher than those of irrigated crops. The SAFER determines the evapotranspiration of the crop (Etc) in two steps, using the Kc crop coefficient and evapotranspiration of the reference crop (ETo). The input data is multispectral and thermal images along with weather data.

The SAFER algorithm is widely used and has been validated in several regions of Brazil and the world, primarily through satellite data. However, references involving UAV data remain scarce and are still under development. Our hypothesis is that multispectral sensors on board UAVs allow the estimation of evapotranspiration with greater spatial and temporal accuracy in different land use and land cover conditions in the Cerrado biome, when compared to estimates based on satellite data and point measurements using the eddy covariance (EC) method. Therefore, the main objective of this study was to estimate evapotranspiration in specific land use types within the Cerrado biome using a multispectral UAV-borne sensor. Specifically, the study aims to (1) estimate ET for three distinct land uses: common bean crops, pasture, and semideciduous seasonal forest; and (2) compare the ET estimates obtained from UAV-based data using the SAFER algorithm with those derived from satellite data and direct measurements using the eddy covariance method.

Materials and methods

Study location

The research was conducted at Fazenda Capivara, an experimental property of Brazilian Agricultural Research Corporation (Embrapa), located in the municipality of Santo Antônio de Goiás, State of Goiás (latitude of 16° 30′ 00″ S, longitude of 49° 17′ 30″ W and altitude of 823 m) (Fig. 1). The predominant soil in this region is classified as a typical Acriferric Red Latosol, with a clayey texture (~ 530 g kg^{-1} clay) in flatter relief. According to the Köppen classification, the climate in this region is Aw—tropical savanna, with dry winter (May to September), minimum temperature around 16 °C (between June and July), rainy summer (October to April), and average annual temperature of 22.6 °C. The average annual rainfall is 1505 mm. The maximum average relative humidity is around 80% in the rainy season (December, January, February, and March), coinciding with the planting season; in August and September, the relative humidity can reach a minimum of 20%, with an average of around 50%. The average daily insolation in the region, between September and April, is between 4 and 7 h, while from May to August, the daily average can exceed 8 h (Stone, 2006).

The methodology consisted of the acquisition and processing of data from four sources: direct measurements with the eddy covariance (EC) method, satellite, meteorological data, and UAV, to evaluate the SAFER algorithm and produce ET maps for the three land uses (common beans, pasture, and semideciduous seasonal forest), as shown in the flowchart (Fig. 2). We initially intended to use satellite data from Landsat 8, but the intense cloud cover during the selected period, typical of the Cerrado biome, made this impossible. Therefore, we focused on using data from the Sentinel satellite instead. Data from the flow tower will be compared with satellite data from Sentinel (10 m spatial resolution) and UAV data with a spatial resolution of 5.5 cm. In the area implanted with common beans (*Phaseolus vulgaris* L., cultivar BRS FC 104), it is an iLP system since the 1999/2000 agricultural harvest. In this harvest analyzed (2021/2022), sowing was carried out in a no-tillage system on October 26, 2021, and harvested on January 15, 2022.

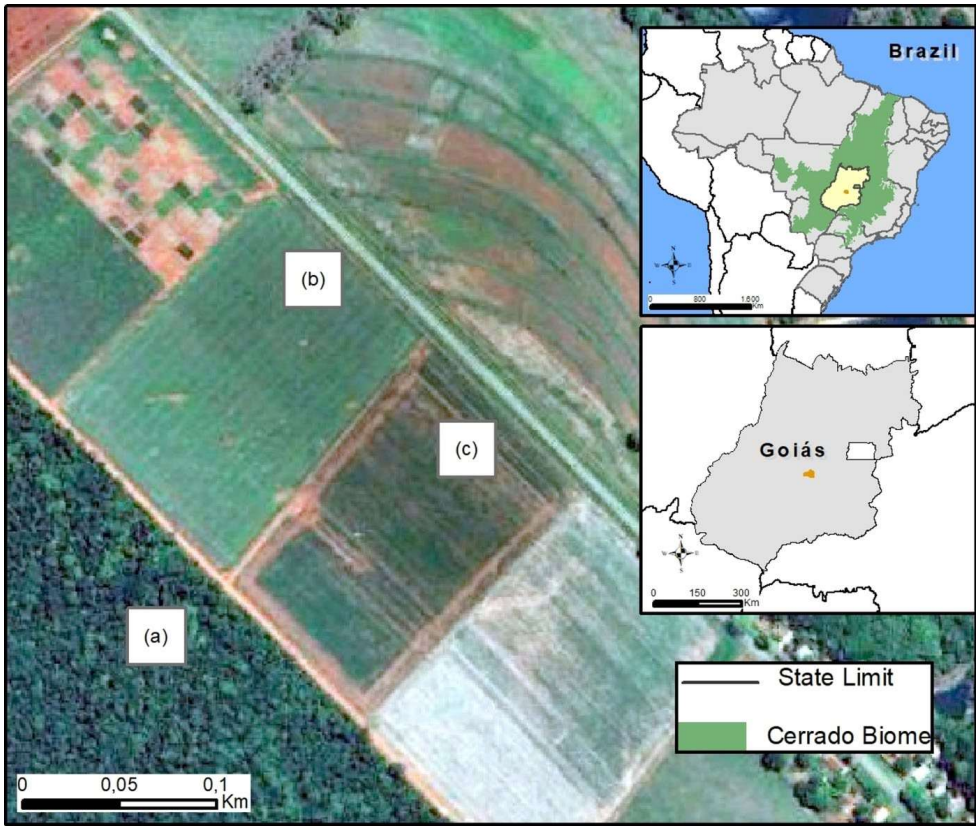

Fig. 1 Study site geographic location: Santo Antônio de Goiás, in the state of Goiás, Brazil. True-color PlanetScope image (R = B3, G = B2, NIR = B4) from June 2020, UTM Zone 22S (EPSG: 32,722), showing marked land use classes: **a** forest, (**b**) pasture, and (**c**) common bean cultivation for the 2021/2022 crop year

Satellite image acquisition and processing

For this study, we used data from the Sentinel-2 satellite, which offers publicly accessible, medium-to-high spatial resolution, essential for analyzing evapotranspiration and correlating it with field and UAV data. The Sentinel-2 imagery, orbit/point 22/KFG, was obtained through the ESA/Copernicus portal (https://scihub.copernicus.eu/dhus/#/home) and processed on the R platform using a custom script. This processing included atmospheric correction to convert the DN values into top-of-atmosphere radiance and reflectance (Eqs. 1 to 4).

Digital number (DN) satellite data were converted to spectral radiance for each band (Eq. 1).

$$L\lambda = \left(\frac{L_{MAX} - L_{MIN}}{255}\right) Q_{CAL} + L_{MIN} \quad (1)$$

where

LMAX maximum radiance (W m^{-2} sr^{-1} μm^{-2});
LMIN minimum radiance (W m^{-2} sr^{-1} μm^{-2});
Qcal pixel intensity (ND), integer from 0 to 255.

The reflectance data were generated from the radiance values (Eq. 2).

$$P\lambda = \frac{\pi \times L\lambda}{ESUN_{\lambda} \times cosZ \times E_0} \quad (2)$$

where

$L\lambda$ radiance of each band;
SUN λ spectral irradiance at the top of the atmosphere;
cosZ zenith angle;
E_0 daily angle;

where E_0, wich is referred to in Eq. 2, is defined by Eq. 3.

$$E_0 = 1.000110 + 0.0342221\ cos(da) + 0.001280\ (da) + 0.000719\ (2 \times da) + 0.000077\ sin\ (2 \times da) \quad (3)$$

where "da": daily angle.

Being "da" defined by Eq. 4:

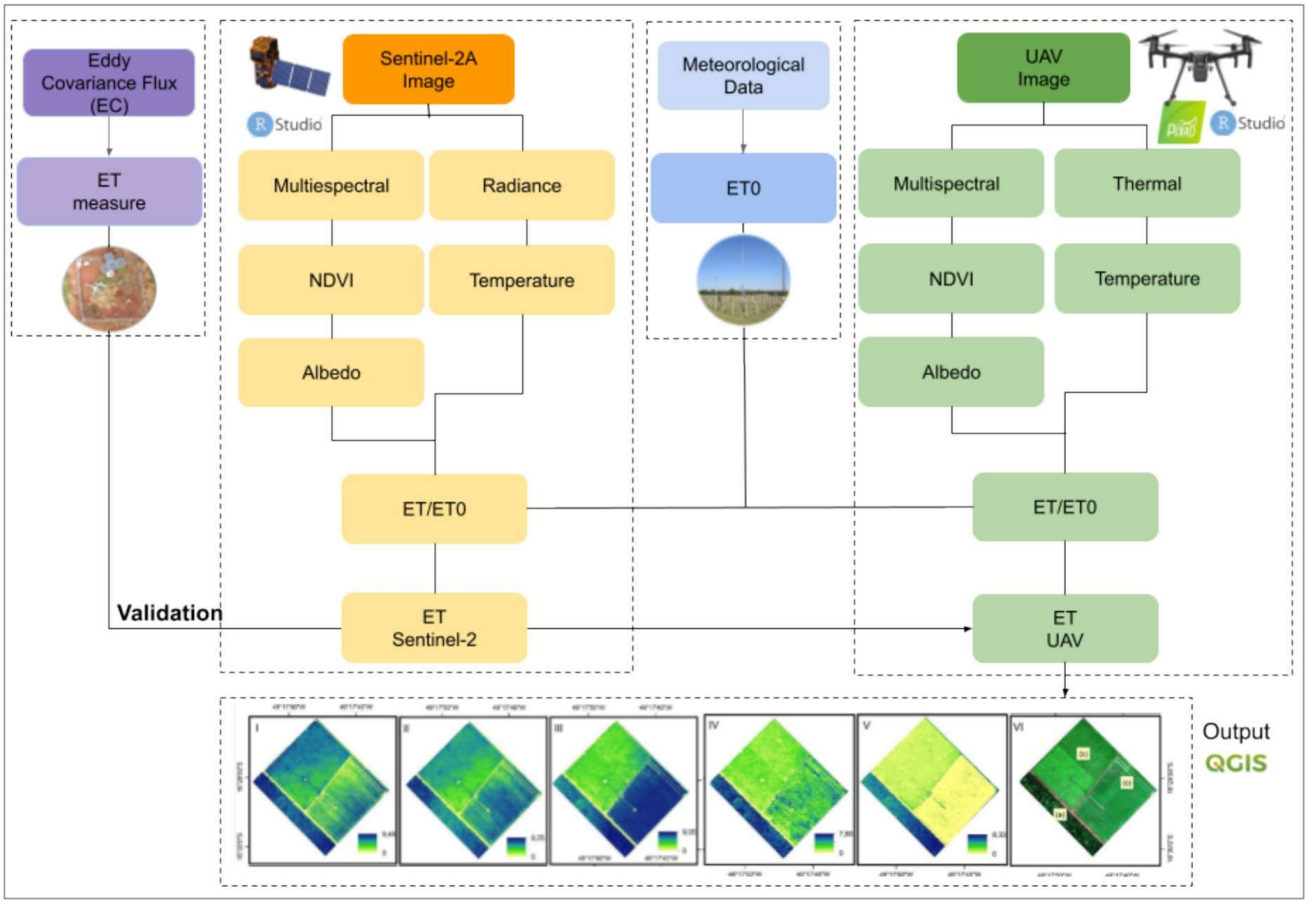

Fig. 2 Flowchart showing the methodology adopted for evaluating the SAFER algorithm using data from satellite, UAV, and direct measurements with the eddy covariance (EC) method and generating ET maps for different land uses (common beans, pasture, and semideciduous seasonal forest)

(a) (b)

Fig. 3 Equipment **a** Matrice 200 UAV and **b** MicaSense Altum imaging sensor, accompanied by the DLS sensor

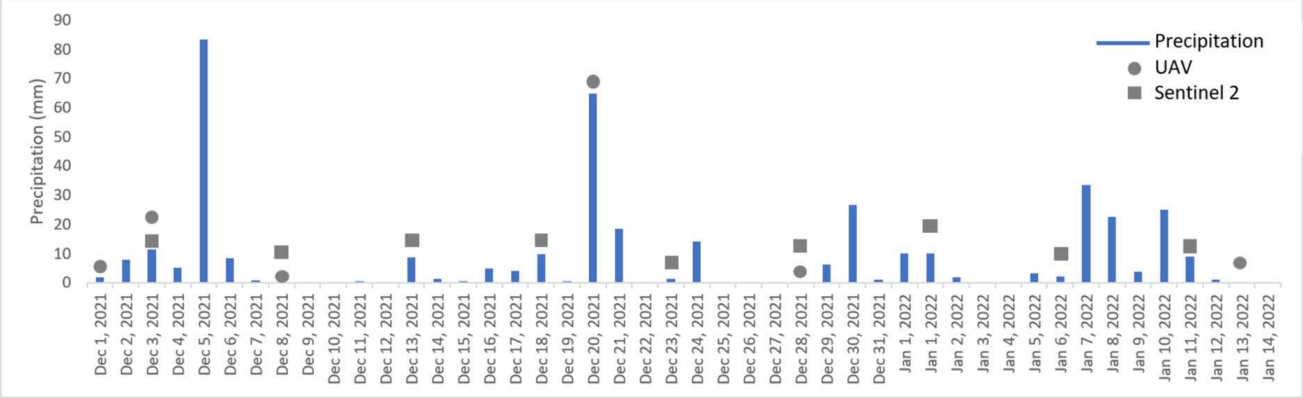

Fig. 4 Precipitation and the dates of satellite and UAV data collection at the study site located in Santo Antônio de Goiás, in the state of Goiás, Brazil

$$da = \left(d_n - 1\right)\frac{2\pi}{365} \tag{4}$$

where d_n: Julian day of the image.

Acquisition and processing of UAV images

To conduct this study, we used a rotary-wing UAV, quadcopter, manufactured by DJI, model Matrice 200, embedded with a Downwelling *Light Sensor* (DLS) to correct the luminosity and provide GPS data, and multispectral imaging sensor of the MicaSense Altum brand (MicaSense Inc., Seattle, USA) (Fig. 3a, b). Its five multispectral bands with the respective band center and bandwidth are as follows: Blue 475 nm (20 nm), Green 560 nm (20 nm), Red 668 nm (10 nm), Red Edge 717 nm (10 nm), and NIR 842 nm (40 nm), in addition to a thermal infrared sensor (LWIR) centered at 11,000 nm. In all, there were six missions with this UAV, as detailed in Fig. 4, between December 1, 2021, and December 14, 2022.

Flight planning was carried out with Pix4D capture *software*, where the flight height of 120 m above the ground was defined, with 75% frontal and lateral overlap of the photos, guaranteeing a GSD (*ground sampling distance*) of 5.5 cm. Flights were always executed from 10:00 am to 11:30 am. Prior to each flight, images were captured of a calibrated black-and-white reference panel from the nadir perspective to facilitate the calibration of the multispectral camera lenses. This calibration step is essential to ensure that the reflectance values derived from the UAV images are accurate and comparable to satellite-based measurements, thereby standardizing the radiometric quality of all datasets. The images collected during the flights were processed in Pix4D Mapper (version 4.4.12), resulting in a dense point cloud and the creation of a digital elevation model (DEM), which was then used to automatically generate orthomosaics at the reflectance level.

Acquisition of weather data

The reference evapotranspiration (ET0; mm day^{-1}) was calculated using the FAO Penman–Monteith standard method (Allen et al., 1998); for this purpose, meteorological data were obtained from the Embrapa Arroz e Feijão station, located in the municipality of Santo Antônio de Goiás—GO (latitude 16° 28′ 00″ S, longitude 49° 17′ 00″ W and altitude of 823 m). This station is located within a 1.2 km radius of the experimental field, comprising data on solar radiation, air temperature, relative humidity, precipitation, and wind speed. The accumulated rainfall in the analyzed period (December 1, 2021, and January 14, 2022) was 473.8 mm. Daily precipitation, flight dates, and satellite image acquisition dates are shown in Fig. 4.

Mapping evapotranspiration by the SAFER model

The SAFER model, unlike more complex evapotranspiration estimation models, does not require hot and cold pixel input. It provides the ET/ET0 ratio and uses canopy characteristics, temperature, surface albedo, and meteorological data to estimate the crop coefficient (Kc), which can be converted to current

ET. This model was initially developed for satellite imagery; therefore, distinct methodologies for surface albedo and surface temperature for satellite and UAV data will be presented.

ET maps were generated for each image mosaic obtained by UAV and also by satellite (cloud-free scenes) using the SAFER algorithm (Teixeira, 2012) (Eq. 5), with parameters calibrated in the RStudio software (RStudio, Boston, USA). Based on the following parameters: surface albedo (α_0), surface temperature (T_0), and normalized difference vegetation index (NDVI) (Rouse et al., 1973). The NDVI is used in the SAFER algorithm due to its effectiveness in representing vegetation cover and its correlation with ET. By distinguishing areas of dense, healthy vegetation with higher NDVI values, the algorithm can better estimate water usage through ET. NDVI also helps model the fraction of radiation absorbed by vegetation (fPAR), which is crucial for calculating ET. Its simplicity, requiring only two spectral bands (red and near-infrared), and widespread availability from satellite imagery make NDVI an efficient and practical choice for estimating ET in the SAFER model. Images were used as remote sensing input data and ET_0 by weather station data.

$$\frac{ET}{ET_0} = exp\left[a + b\left(\frac{T_0}{\alpha_0 \times NDVI}\right)\right] \tag{5}$$

ET_0 is the reference evapotranspiration obtained by the Penman–Monteith method and the regression coefficients $a = 1$ (Hernandez et al., 2014; Teixeira et al., 2013) and $b = -0.008$ (Teixeira, 2010).

The surface albedo had different calculation procedures for Sentinel-2 satellite images (Eq. 6) and for UAV (Eq. 9).

$$\alpha_0 = 0.7 \times \alpha_{top} + 0.06 \tag{6}$$

where α_{top} is the albedo obtained at the top of the atmosphere (Eq. 7).

$$\alpha_{top} = \sum(\omega_p \times p_\lambda) \tag{7}$$

where.

p_λ = reflectance.

ω_p = calibration coefficient of each band, according to Eq. 8:

$$\omega_\lambda = \frac{ESUN_\lambda}{\Sigma ESUN_\lambda} \tag{8}$$

Unlike obtaining the albedo for satellite images, UAV images do not consider the albedo of the top of the atmosphere. The weights for each band are obtained according to Planck's law (Teixeira, 2010), and then all bands are added (Eq. 9).

$$\begin{aligned}\alpha \;=\; & 0.24\ (\text{Blue}) + 0.23\ (\text{Green}) + 0.2\ (\text{Red}) \\ & + 0.14\ (\text{NIR}) + 0.18\ (\text{Red Edge})\end{aligned} \tag{9}$$

The daily land surface temperature (LST) was estimated as a residual in the daily radiation balance (Eq. 10) (Silva et al., 2019; Teixeira et al., 2014b, 2015).

$$LST = \sqrt[4]{\frac{R_G S - a_0 R_G + \varepsilon_A \sigma T_a^4 - R_n}{\varepsilon_s \sigma}} \tag{10}$$

where R_n is the daily net radiation; ε_a and ε_s are the atmospheric and surface emissivities, respectively; and σ is the Stefan–Boltzmann constant (5.67×10^{-8} W m^{-2} K^{-4}).

The surface emissivity and atmospheric emissivity were calculated by Eqs. 11 and 12.

$$\varepsilon_A = \varepsilon_A(-ln\tau_{sw})^{b_A} \tag{11}$$

$$\varepsilon_S = a_S ln(NDVI) + b_s \tag{12}$$

where sw is the shortwave atmospheric transmissivity calculated as the ratio of RG to the incident solar radiation at the top of the atmosphere (Teixeira et al., 2015) and $a_A, b_A, a_s, and a_s$ are regression coefficients 0.9634, 0.1135, 1.0035, and 0.0589 (Teixeira, 2010; Teixeira et al., 2014a). The regression coefficients in Eq. 13 are between those obtained for Idaho (a_A = 0.85 and $b_A = 0.09$ (Allen et al., 2000)) and Egypt (a_A = 1.08 and $b_A = 0.26$ (Bastiaanseen et al., 1998)).

The net radiation (R_n) was calculated using the Slob equation (Teixeira et al., 2014a, 2014b):

$$R_n = (1 - a_0)R_G - a_L \tau_{sw} \tag{13}$$

The coefficient a_L can be found through its relationship with T_a according to Eq. 14.

$$a_L = cT_a - d \tag{14}$$

where c and d are regression coefficients found to be 6.99 and 39.93 (Teixeira et al., 2008), respectively.

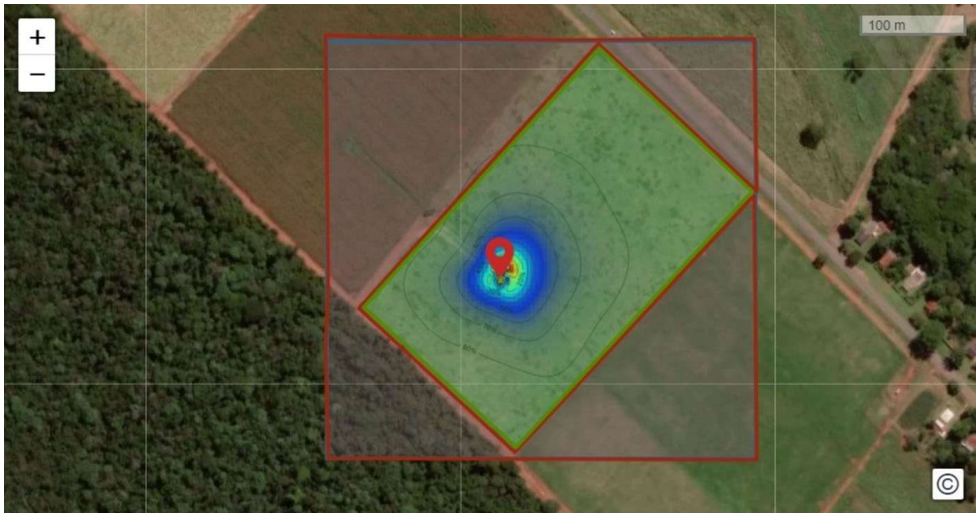

Fig. 5 Study site geographic location: Santo Antônio de Goiás, in the state of Goiás, Brazil. The true-color Google Earth image from 2021, in EPSG: 4326—WGS84, was used as the base map. Additionally, the footprint contribution area of the eddy covariance (EC) method was overlaid to analyze the influence of the surrounding land cover on the evapotranspiration measurements

The normalized difference vegetation index (NDVI) was calculated by Eq. 15.

$$NDVI = \frac{(\rho_{nir} - \rho_{red})}{(\rho_{nir} + \rho_{red})} \quad (15)$$

where ρ_{nir} and ρ_{red} are the reflectances in the NIR and Red bands, respectively.

The instantaneous values of the ET/ET_0 ratio (Eq. 1) were multiplied by the daily values of ET_0 calculated by the Penman–Monteith method, resulting in daily evapotranspiration (Eq. 16):

$$ET_a = \frac{ET}{ET_0} \times ET_0 \quad (16)$$

where ET_a is the current evapotranspiration (mm day^{-1}) and ET_0 is the reference evapotranspiration (mm day^{-1}) calculated by the Penman–Monteith method.

Reference evapotranspiration (ET_0) was standardized by the FAO Penman–Monteith method (Allen et al., 1998) (Eq. 17).

$$ET_0 = \frac{0.408\Delta(R_n - G) + \gamma\frac{900}{T+273}u_2(e_s - e_a)}{\Delta + \gamma(1 + 0.34u_2)} \quad (17)$$

where ET_0 is the reference evapotranspiration (mm day^{-1}), R_n is the radiation balance (MJm^2day^{-1}), G is the heat flux in the soil (MJm^{-2} day^{-1}), T is the average daily temperature at 2 m height (°C), u_2 is the wind speed at 2 m height (ms^{-1}), e_s is the vapor saturation pressure (kPa), e_a is the actual vapor pressure (kPa), γ is the psychrometric factor, and Δ is the slope of the saturation vapor pressure curve (kPa $°C^{-1}$); 0.408 corresponds to $1/\lambda$, with λ being the latent heat of evaporation of water, equal to 2.45 MJ. Kg^{-1} at 20 °C; 900 is a coefficient for the reference culture (kJ^{-1}.kg. $K.d^{-1}$), which involves constant values of the equation.

Acquisition and processing of eddy covariance (EC) data

The performance of the SAFER algorithm was analyzed for UAV data based on field data from a flow tower (Li-Cor LI-7500), with ET obtained by the eddy covariance (EC) method. The tower contribution area (*footprint*) (Fig. 5) was calculated using the Tovi Footprint Analysis methodology (Kljun et al., 2015) based on the following inputs: instrument height, crown height, wind speed, desired distances from the tower, friction speed, and displacement from the zero plane. Of these, the model calculates how much of the measured flow comes from a given distance. The initial radius of coverage plotted was 100 m from the tower. The maximum contribution comes from a closer distance upwind. More than 80% of the measured flows come from an area within 80 m of the tower. In Fig. 5, the *footprint* contour lines are shown in 10% intervals, from 10 to 80% from the red marker representing the tower. This contribution interval was used to remove ET values from UAV

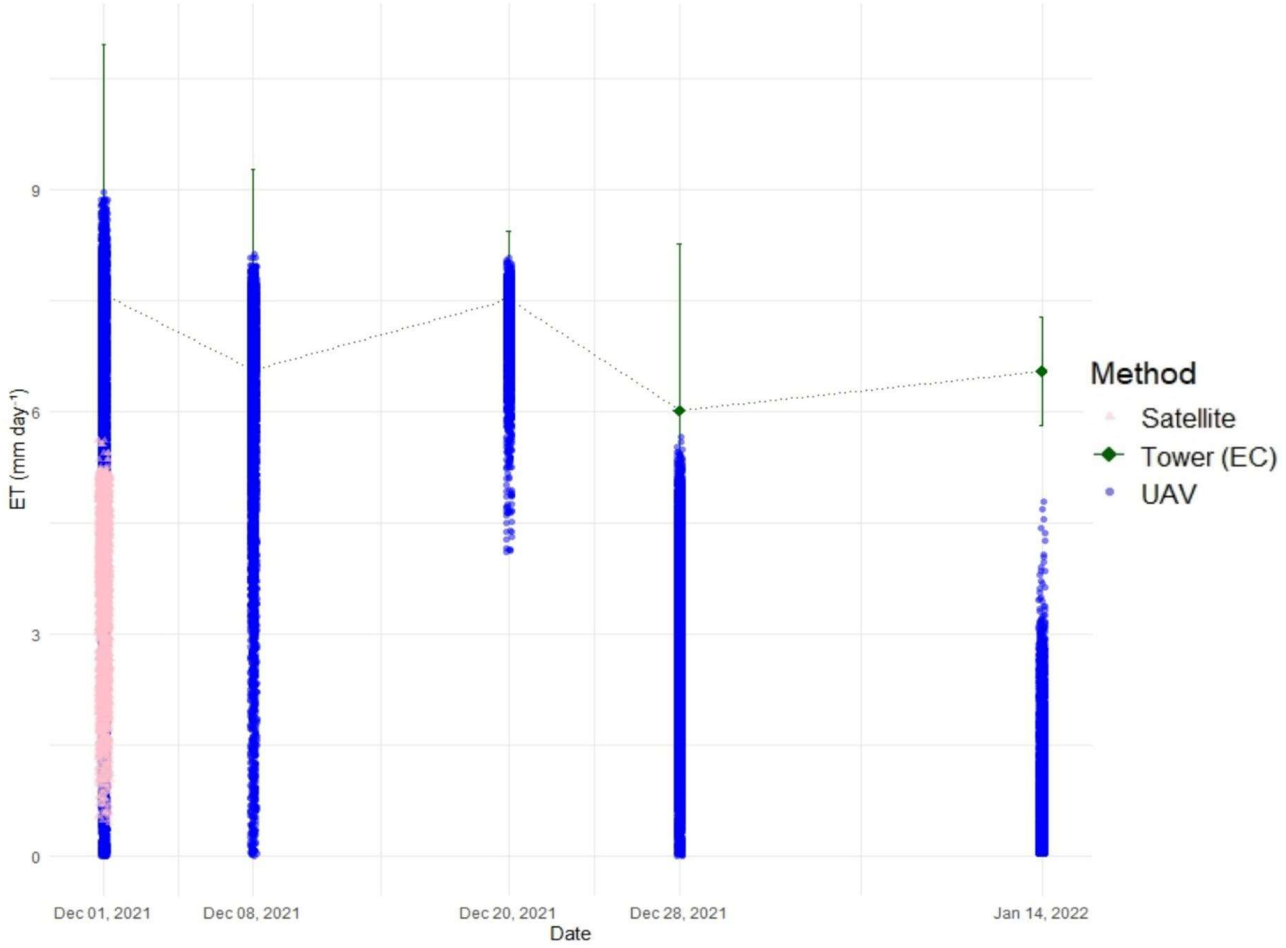

Fig. 6 Comparison of evapotranspiration (ET) in mm day^{-1} based on the three sources: satellite, UAV, and eddy covariance (EC) for the early, middle, and late seasons of common bean cultivation was conducted at the study site located in Santo Antônio de Goiás, in the state of Goiás, Brazil. The data from each source were analyzed to assess the differences in ET estimates throughout the different growth stages of the common bean crop

pixels. The *footprint* of the EC is the experimental area with common bean cultivation, thus not representing the plots with pasture and the semideciduous seasonal forest.

Analysis of evapotranspiration estimation by SAFER algorithm

ET based on UAV data was assessed against flow tower (EC) and Sentinel-2 satellite data. For the EC, the daily ET values (mm day^{-1}) and the ET pixels of the UAV present in the tower *footprint* were compared. The analysis with Sentinel-2 data involved the visual interpretation of the maps generated by the UAV, comparing it with the maps obtained by satellite. In addition, the SAFER algorithm and its input parameters (NDVI, temperature, and albedo) were directly compared to the satellite data on a pixel-by-pixel basis. For the statistical evaluation of these data, we performed a linear regression analysis considering the coefficient of determination (R^2) and the mean square error (RMSE) indicators (Eqs. 18 and 19).

$$R^2 = \left[1 - \frac{\sum(y-\hat{y})^2}{\sum(y-\hat{y})^2}\right] \tag{18}$$

$$RMSE = \sqrt{\frac{\sum_{i=1}^{n}\left(y-\hat{y}\right)^2}{n}} \tag{19}$$

where n is the number of observations, y is the i-th prediction, and $\hat{y}$ is the i-th observation.

Results and discussion

Evaluation of ET based on UAV, Sentinel-2, and eddy covariance (EC)

Within the area covered by the EC method are located thousands of pixels of UAV images that represent the ET of both the plant and the soil. However, the EC coverage is limited to the common bean crop area, as the pasture and forest areas do not have EC measurements. Therefore, the comparison described in Fig. 5 is focused solely on the common bean crop. In dates of full vegetative development of the common bean (mid-cycle, on December 8 and 20, 2021), the behavior of UAV-based ET corresponds to that obtained via EC, with close averages (Fig. 6). Just after the sowing event, when the canopy is not yet fully covering the soil and just before harvest, when plants are in senescence, the ET determined via UAV is underestimated. The ET determined via Sentinel-2 was underestimated with respect to EC and UAV, probably due to the cloudy atmosphere.

The underestimation of ET when using remote sensing has been observed by several authors, especially in periods when there is an influence of soil or straw covering the soil (Chen et al., 2014; Pan et al., 2018; Sales et al., 2016; Ye et al., 2022), which is a common situation under crop-livestock systems in the Cerrado. To overcome this problem, it is suggested to evaluate the ET of an area from more than one source of data, or in a dual mode, which should include plant and soil pixels. Remote sensing ET models can be divided into two main categories, single source and dual source, which differ in the approach used to consider the interaction between soil, vegetation, and atmosphere (Paul et al., 2014). In the single-source model, soil and agricultural vegetation are treated as a single component, while in the dual-source model, they are separated, based on vegetation indices (French et al., 2015).

All pixels within the tower's area of influence were evaluated together, as we recognized that the ET behavior reflects the functioning of the soil–plant-atmosphere system. This includes considerations about the average being potentially reduced due to soil influence at the beginning of the crop cycle and senescence during the final stages of the crop. The proposed method, SAFER, uses NDVI, albedo, and temperature values measured directly from the target, with reduced atmospheric influence. ET values were expected to be reduced with decreasing NDVI (indicating lower vegetation cover) and increasing albedo and soil temperature. This is because denser vegetation cover results in greater evapotranspiration due to plant transpiration, while lighter surfaces (high albedo) and high soil temperature tend to have low ET, with direct evaporation of soil water being lower. As a result, the average evapotranspiration is reduced in these areas. The EC method assesses energy fluxes in the atmosphere, including sensible heat and latent heat flows, which are influenced by the interaction between the Earth's surface and the atmosphere (Yazbeck et al., 2024). It is reasonable to expect that ET values estimated by SAFER will be more sensitive to changes in soil characteristics than measurements made by EC, which assess energy flows in the atmosphere.

Analysis of UAV-based SAFER and Sentinel-2 factors

The spatial resolution of the UAV images was degraded to the spatial resolution of the Sentinel image, and then each pixel was evaluated with its corresponding pixel. The linear relationship was assessed with all pixels of the study area, for the set of classes of uses evaluated (Figs. 7 and 8). The data obtained by UAV for ET, NDVI, temperature, and albedo demonstrated significant efficacy, with a high level of significance ($p < 0.001$) for all parameters analyzed. These results show a robust relationship for ET ($R^2 = 0.84$, RMSE = 0.68 mm day^{-1}) when compared to Sentinel-2 data, while the NDVI also presented a strong correlation ($R^2 = 0.82$), confirming the accuracy of UAV data in capturing vegetation indices. The temperature showed an intermediate correlation ($R^2 = 0.51$), indicating some variability in comparison with the Sentinel-2 data. The albedo was the parameter with the lowest ratio ($R^2 = 0.38$). It is noted that this parameter, when obtained by UAV, exhibits significant spatial variation. The SAFER algorithm was evaluated for UAV data taking Sentinel-2 satellite data as a reference. Teixeira (2012) performed a simplified linear relationship between daily ET measured in the field and satellite, reaching a correlation ratio of $R^2 = 0.80$ and validating satellite data for the SAFER application.

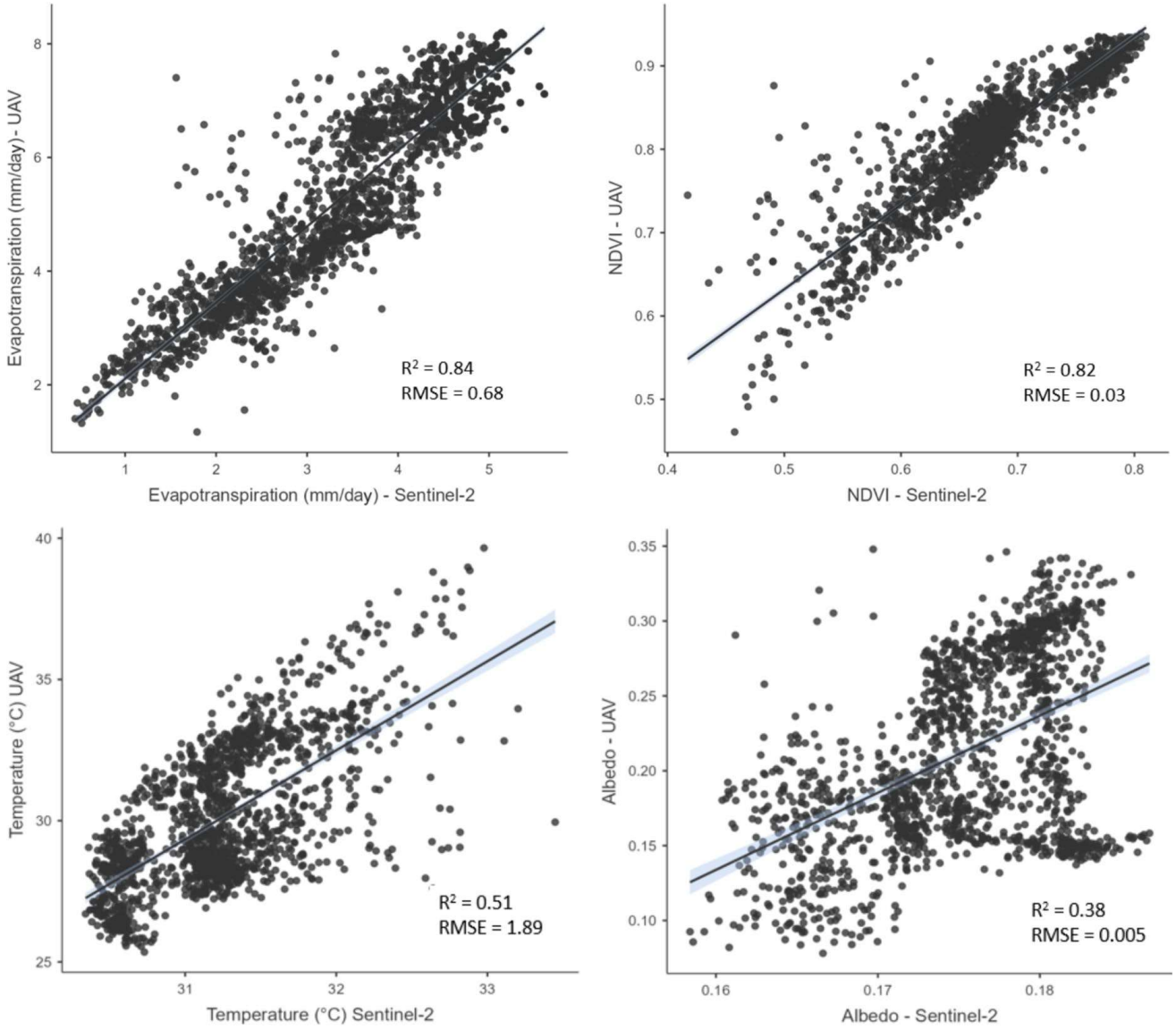

Fig. 7 Correlations among evapotranspiration (ET), normalized difference vegetation index (NDVI), surface temperature, and albedo calculated with satellite (Sentinel-2) and UAV methods, from common bean crop and pasture (in crop-livestock system) and a native semideciduous seasonal Cerrado forest. The different vegetation cover types are not individually indicated in the graphs

The albedo, NDVI, temperature, and ET generated with UAV and Sentinel-2 methods are shown in Fig. 8. In general, the UAV data showed a higher distribution and higher averages in relation to the parameters calculated with satellite data.

On the other hand, the Sentinel-2 data demonstrate a more uniform consistency, varying according to different soil cover, but remaining stable within the same type of cover: pasture, crop, and native forest. The three types of soil cover analyzed area heterogeneous, which results in greater spectral confusion when confronted pixel by pixel, given the range in spatial resolution between satellite (10 m) and UAV (5.8 cm). In the UAV images, regions of exposed soil bring extremely low values when compared to satellite data, which, due to the pixel size, confounds exposed soil and vegetated areas, causing greater spectral confusion, with rare pixels of pure representation of exposed soil. The greater the number of pixels evaluated (where low values represent evaporation and not transpiration), the more abundant outliers become (Mokthari et al., 2021). When analyzing

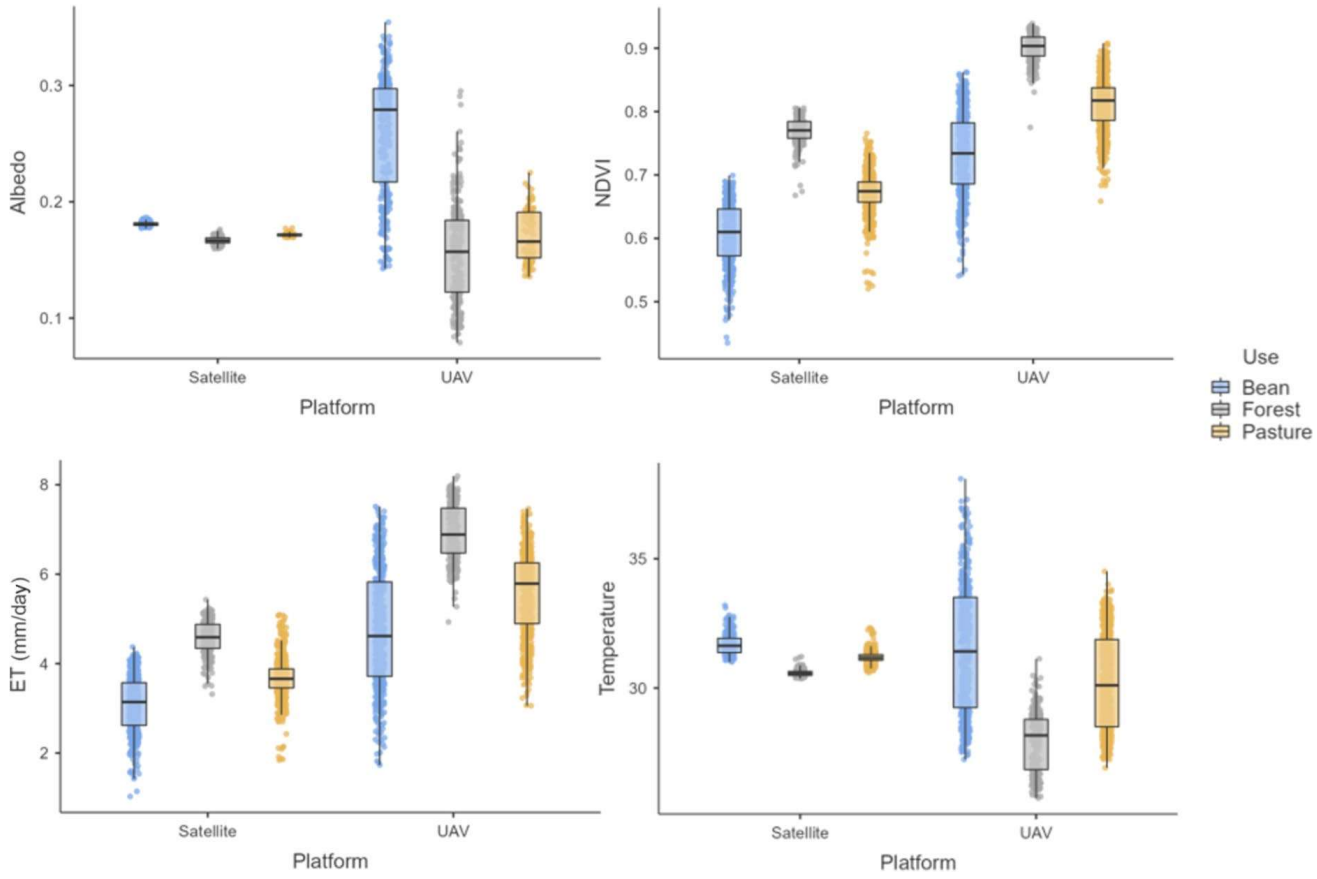

Fig. 8 Comparison of albedo, NDVI, temperature, and ET parameters obtained with the SAFER algorithm for UAV and satellite images (Sentinel-2), in common bean and pasture in crop-livestock system and a native semideciduous seasonal Cerrado forest

the high-resolution image captured by the sensor on board the UAV, we noticed that satellite images have some limitations in identifying specific targets due to their spatial resolution. This was mainly evidenced in the information on temperature and albedo and can result in the distortion of values due to the influence of other elements, which in turn can generate negative interferences in the radiance recorded by the images, making it difficult to overall evaluation.

Albedo exerts a significant influence on the energetic interaction between the biosphere and the atmosphere (Kalnay et al., 1996). In turn, the types of land cover that reflect a greater share of shortwave radiation end up having less energy to sustain the hydrological cycle (Caioni et al., 2020). Figure 9, which spatializes the results and allows for better visualization, shows that the albedo remained almost unchanged in the Sentinel-2 images, with values around 0.18 (Fig. 8). In contrast, the UAV data showed significant variation in albedo, especially between different soil covers. The higher albedo in UAV images is associated with higher spatial resolution of multispectral scenes, which caused greater influence of bare background soil. The lowest albedo value was obtained for the native forest, followed by pasture and common bean cultivation (highest albedos). Low albedo in native forest areas is expected, given its dark green and closed canopy, as well as the greater soil coverage, without interference from these in the measurements obtained with the multispectral images. The common bean crop was in the vegetative stage, with some soil exposure, while the pasture provided, at the date of data acquisition, was conserved with little influence from the background soil.

The NDVI presented outliers for both methods (UAV and satellites), however with a higher median and greater distribution of pixel values for the UAV. Santos et al. (2021), analyzing the performance of the NDVI against Landsat 8 and Sentinel-2, also observed the greater variability of this index with

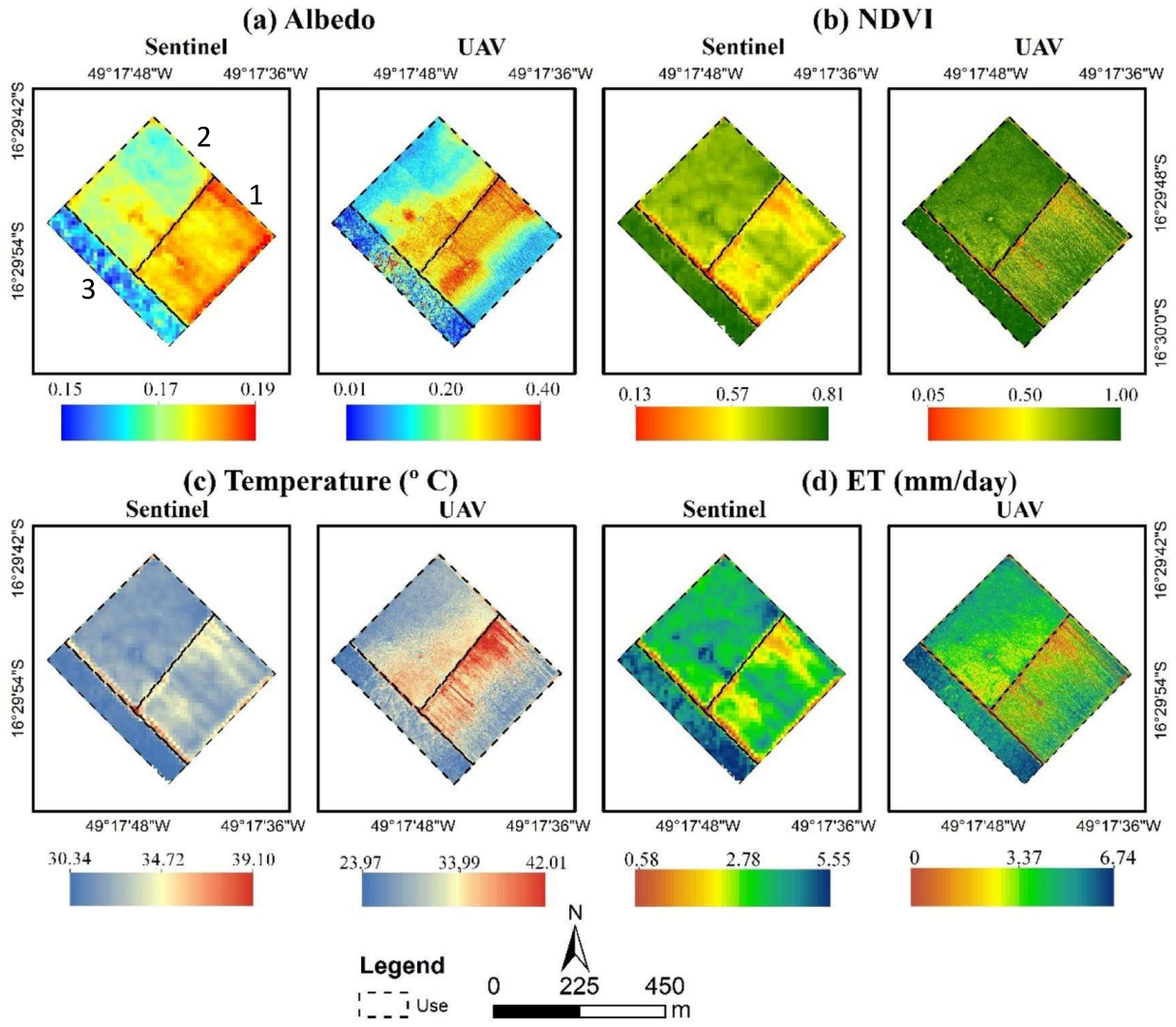

Fig. 9 **a** Albedo, **b** normalized difference vegetation index (NDVI), **c** surface temperature, and **d** evapotranspiration (ET) from data obtained by satellite (Sentinel-2) and UAV in common bean crop under no-till (1) and pasture (2) in a crop-livestock system and a native semideciduous seasonal Cerrado forest (3)

UAV images compared to said satellites. A presence of outliers is observed in the satellite-derived temperature data, which may be related to areas of exposed soil or straw. Surface emissivity and atmospheric corrections play an essential role in the assessment of surface temperature, which consequently significantly influences the quality of data obtained through remote satellite measurements. When it comes to UAV data, due to the proximity to the surface, atmospheric interference is attenuated, so these data tend to be more representative of land use and land cover variation.

Considering the input parameters, the ET (Fig. 8) estimated by satellite showed less variability within the examined areas compared to the ET calculated by UAV, showing lower averages. The ET graph indicates similar behavior to NDVI, but with greater symmetry between ET-UAV and NDVI-UAV. Cihlar et al. (2000) found a 0.60 correlation between ET and NDVI. Mokthari et al. (2021) obtained a strong linear relationship ($R^2 = 0.72$) between them.

When analyzing the data obtained by both sets of sensors (aerial and satellite), there is a difference in the dispersion of data from the UAV and Sentinel-2 for the parameters (Figs. 8 and 9) of albedo, NDVI, temperature, and ET, in different classes of land use, showing a distinct capacity in relation to spatial resolution and sensitivity in capturing variations in the different indexes and contexts of the landscape. Thus,

for the albedo, NDVI, and temperature parameters, the UAV demonstrates a more pronounced dispersion among the three land use classes. However, for ET, the UAV presents an even more pronounced dispersion. The enlarged dispersion of the ET-UAV data may indicate two distinct features. On the one hand, it suggests superior sensor sensitivity, allowing the UAV to detect subtle variations in terrain where the Sentinel-2 spatial resolution does not. On the other hand, UAV has more noise and greater susceptibility to outliers and median displacement.

This phenomenon can be attributed to the complex interaction between spatial resolution, inherent terrain heterogeneity, and the specific sensitivity of the SAFER model to different input parameters. Notably, the combinatorial process of these parameters in the calculation of ET can attenuate certain variabilities in the UAV, while potentiating discrepancies observed in Sentinel-2. Independently of the sensor used, results of albedo, NDVI, ET, and temperature showed similar patterns in the different types of land use (Fig. 7). In other words, the area under native forest showed the lowest albedo and temperature and highest NDVI and ET, followed by the areas under common bean crop and pasture. Using simulated land cover maps of Eastern Amazonia, Brazil, a similar pattern was also reported for the rainforest, soybean crop, and pasture areas, indicating an association of reduction in precipitation with increase in albedo and diminution of ET (Sampaio et al., 2007). The authors have reported that pasture and soybean crops show lower surface aerodynamic roughness, lower leaf area indicated by NDVI values, and shallower rooting depth compared to the forest. Recent research for a Neotropical Savanna (the Brazilian Cerrado) suggests that reduction in regional evapotranspiration at the beginning of the wet season potentially contributed to the decrease in rainfall (Hoffmann et al., 2023). The beginning of the wet season, October and November, is the recommended sowing time of most rainfed grain crops like common bean.

Differences between UAV and Sentinel-2 in spatial resolution

Regarding albedo (Fig. 9a), Sentinel-2 images processed for this purpose revealed a color variation, from light blue to dark red, indicating lower and higher albedo values, respectively. The albedo scale between Sentinel-2 and UAV was well differentiated. While in Sentinel-2, there is a small variation, of 0.04%, with the UAV a higher variation was obtained, demonstrating a greater spatial distribution capacity of the albedo. In addition, UAV images provide greater definition capacity and sharper contrast, ensuring better visual analysis of the distribution of this physical variable.

With NDVI, values close to 1 indicate denser and healthier vegetation, while yellow and red shades suggest sparse and/or stressed vegetation. In the NDVI obtained with Sentinel-2 (Fig. 9b), this is influenced by the spatial resolution of 10 m, manifesting a greater generalization, with effects of near edge of roads, or buffering areas, which can affect the analyses of productivity and vegetative development and health of the crop. In contrast, the NDVI obtained via UAV demonstrated greater detail. Studies by Cheng et al. (2023) and Zamani-Noor and Feistorn (2022) validate NDVI as a fundamental indicator for monitoring crops, significantly correlating with yields.

In this sense, the detailing of the data generated by UAV, with improved spatial resolution (centimeter), is relevant to evaluate areas with a great diversity of targets, differentiating them, for example, by the presence of exposed soil, gaps in sowing lines, stages of development, texture, and volume of vegetation. Holman et al. (2019) also agree that the ability to capture detailed information about vegetation health, especially in the early stages of cultivation, expands the understanding of plant health. This information is essential to optimize resources, maximize productivity, and reduce environmental impacts.

Regarding the surface temperature (Fig. 9c), a greater amplitude of this parameter was observed with the UAV method, when compared to those of Sentinel-2 highlighting the generalization of the satellite due to its lower spatial resolution for obtaining temperature data, although it still contributes to the mapping of the phenomenon. This resolution results in pixels that reflect the average spectral radiation of the imaged elements, homogenizing the response of the targets contained in this unit on the ground. In turn, UAV stood out in the accurate identification of exposed soils with high temperatures, especially in the pasture and common bean crop, signaling areas with poor development. This perception is corroborated by Santesteban et al. (2017), which emphasize the relevance of thermal images to determine surface

temperature, correlating it to transpiration and, consequently, to the water condition of the crop. According to Sumanta et al. (2020), this analysis is fundamental to assess water stress and anticipate yields.

Regarding ET (Fig. 9d), there was a similarity in the spatial distribution of the index between the Sentinel and UAV images. Additionally, the amplitude of the ET values showed remarkable similarity compared to other indexes previously analyzed. Both platforms effectively detected areas of high evapotranspiration, associated with vegetated zones, as well as zones of reduced evapotranspiration, corresponding to areas devoid of vegetation, with greater detail in the UAV images. This is consistent with the studies by Mokhtari et al. (2021), where they emphasize the ability of UAVs to offer accurate estimates of real evapotranspiration (ETa), especially when employing multi-sensor data fusion techniques. This work also indicates a weak correlation between the evapotranspiration values of the UAV and the Landsat 8 satellite, the latter having a spatial resolution of 30 m.

When analyzing the images obtained by Sentinel-2 and UAV, it is possible to notice significant differences between a satellite image and an aerophotogrammetric orthomosaic, especially in the cartographic detailing obtained with the second method (Fig. 9). The UAV demonstrates a superior ability to identify specific surface details and characteristics, as evidenced by Messina et al. (2020), who highlight that both UAV and satellite images are useful for monitoring agricultural crops, but with different resolutions and objectives, and can be used together or separately as needed. While satellites, such as Sentinel-2, provide a more homogenized view of the landscape due to their larger area per pixel, UAVs, with a higher spatial resolution (on the order of a few square centimeters per pixel), can detect targets in soil or plants, for example, normally missed by satellites.

Sagan et al. (2019) complement this discussion, indicating that early crop stress can be effectively detected using multi-temporal UAV data, merging with satellite observations, and thus overcoming the limitations of satellite remote sensing in crop monitoring. Maitiniyazi et al. (2020) also point to the relevance of UAV images by stating that plant structure characteristics, such as height and density (coverage), derived from these aerial images, are significant indicators for monitoring the growth of agricultural crops.

By evaluating the UAV images in more detail, it is possible to identify nuances, such as minor failures in common bean crops, heterogeneities in pastures, and variations in native Cerrado vegetation, including trees with different shades of green and areas with exposed soil. Gregory et al. (2018) corroborate this perspective, emphasizing that UAV-based plant modeling shows significant advances compared to orbital sensing, especially in terms of greater hits in target identification.

In the recent era of precision agriculture and monitoring, the use of aerial and orbital remote sensing has been fundamental in the acquisition of spatial data for decision-making. The comparison of parameters, such as albedo, NDVI, temperature, and ET, generated from sensors embedded in a satellite (Sentinel-2) or in a drone (UAV) brings light on the best use of technologies to monitor plant development, soil cover, and water or temperature stress generated by land use or soil and crop management. Knowing that the spatial resolution of Sentinel-2 is 10 m and that the images recorded by the UAV have 0.06 m of spatial resolution, one can expect advances in the distribution of the measured variables, in the form of presentation and interpretation by the analysts, including the expectation of saving natural resources from a better understanding of the cultivation area and/or environmental reserve.

Analysis of UAV-based ET values for each land use

According to the descriptive statistical analysis of the data (Table 1 and Fig. 10), it highlighted the presence of pixels with a minimum value of zero for all land uses and dates due to the presence of exposed soil in pasture and beans. For the forest, exposed soil does not appear; however, dry branches and shadow effects reduce the ET values. The ET varied spatiotemporally for each land use (Fig. 10). The highest ET values are in the forest, with mean values ranging from 5.52 to 6.97 mm day^{-1} and a maximum of 9.49 mm day^{-1} within the analyzed period of the rainy season; in the forest, there is also a lower coefficient of variation, indicating that the differences in dossel height did not significantly influence the average pixel variation.

The ET values found in references vary on average between 1 mm day^{-1} in the dry season and 6 mm day^{-1} in the rainy season in forest areas (Oliveira et al., 2005). The forest remained with the

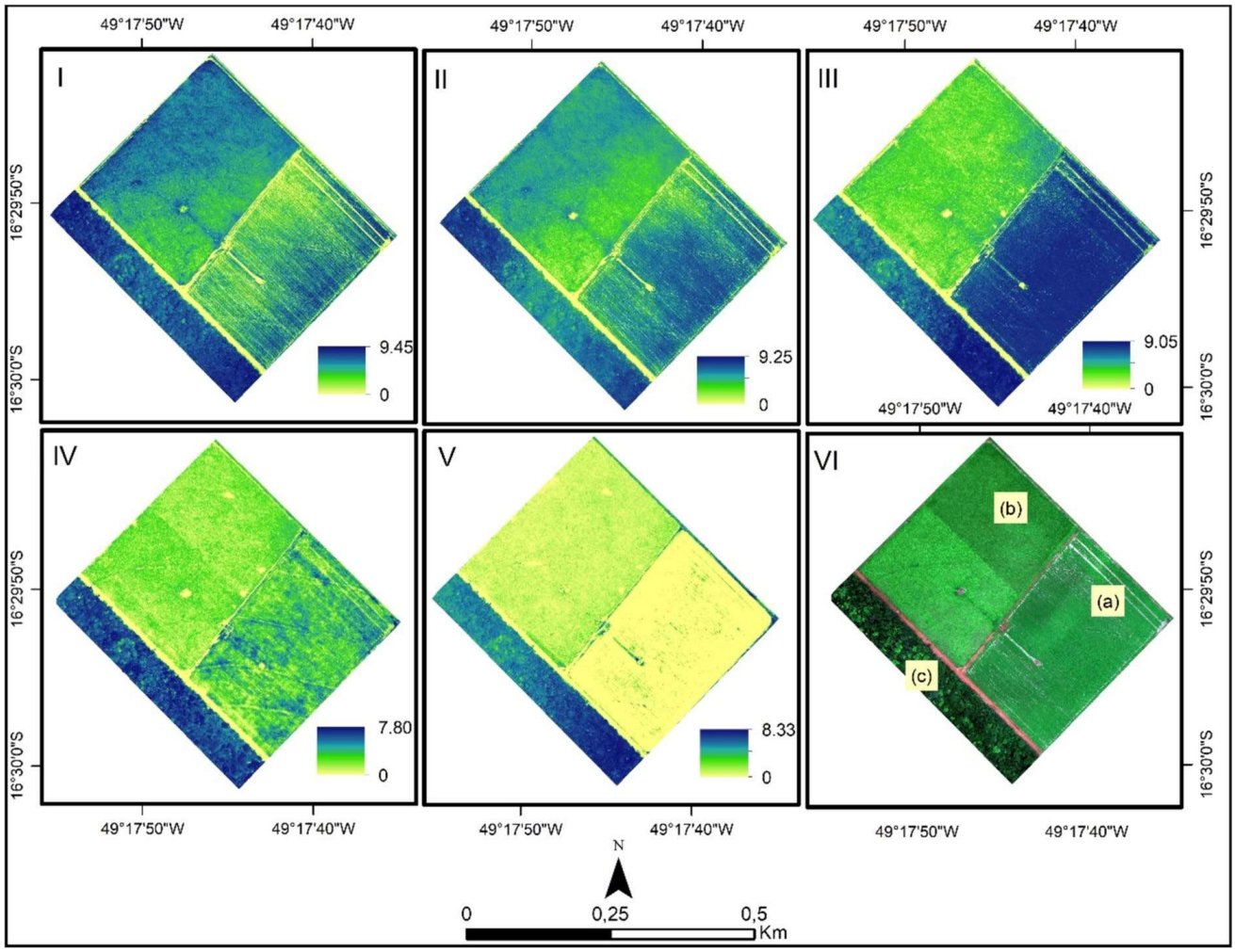

Fig. 10 Evapotranspiration maps (ET, mm day.$^{-1}$) for the dates Dec 1, 2021 (I); Dec 8, 2021 (II); Dec 20, 2021 (III); Dec 28, 2021 (IV); Jan14, 2022 (V) and orthomosaic of use and coverage (VI) with identification of the location of uses: common bean crop under no-till (**a**) and pasture (**b**) in a crop-livestock system and a native semideciduous seasonal Cerrado forest (**c**)

most stable ET throughout the analyzed period. The most expressive changes of ET were noted within the common bean crop and the pasture. Variations are related to soil and crop management of agricultural areas, ranging from bare soil to fully developed canopy (Ruhoff et al., 2012). The ET peak for the common bean crop was precisely at the expected peak of the cultivation coefficient (Kc) (Silva Oliveira et al., 2018). Kc is the relationship between actual crop evapotranspiration (ETc) and reference evapotranspiration (ETo), representing a valuable tool to help farmers determine when and how much to irrigate their crops, ensuring efficient water use and healthy plant growth. In general, Kc values have a regular behavior according to FAO standards (Allen et al., 1998; Doorenbos & Pruitt, 1977), being altered mainly by climatic conditions and whether the crop is irrigated or not, influencing ET behavior. Thus, higher values are expected for irrigated areas, although the water input via precipitation also leads to a considerable increase in ET, as typical for ferralsols of the Cerrado. These soils, especially of finer texture, have high water retention capacity but also are well drained due to their stable microstructure. Micropores also enable capillary water movement from soil to the atmosphere by osmotic differences.

The SAFER model effectively captured ET at high spatial resolution, with results varying according to land use as shown in the spatialization (Fig. 10). In contrast, models such as the High-Resolution

Table 1 Statistical analysis of evapotranspiration (ET) in common bean crop under no-tillage (1) and pasture (2) in crop-livestock system and a native semideciduous seasonal Cerrado forest (3) within the rainy season of the Cerrado biome

Land use	ET (mm day^{-1})	12/01/2021	12/08/2021	12/20/2021	12/28/2021	01/14/2022
Common beans	Min	0.00	0.00	0.00	0.00	0.00
	Max	8.97	8.12	8.07	6.98	4.79
	Average	5.25	6.21	7.35	2.71	0.73
	CV (%)	0.53	0.37	0.25	0.46	0.75
Pasture	Min	0.00	0.00	0.00	0.00	0.00
	Max	8.60	7.87	6.45	3.05	4.88
	Average	4.41	3.43	0.94	0.82	0.71
	CV (%)	0.28	0.37	0.73	0.54	0.67
Forest	Min	0.00	0.00	0.00	0.00	0.00
	Max	9.49	9.24	9.07	7.91	8.33
	Average	6.97	6.81	6.68	5.52	5.81
	CV (%)	0.13	0.16	0.17	0.13	0.18

Mapping of Evapotranspiration (HRMET), Three-Temperature model (3 T), and the Surface Energy Balance Algorithm for Land (SEBAL) present difficulties in estimating ET at such fine scales (Aliabad et al., 2022; Bastiaanssen et al., 1998; Ebert et al., 2022; Lu et al., 2022). These models require the identification of cold and hot pixels in the temperature image, as well as distinguishing between vegetation and exposed soil areas. Without the correct methods, these models may incorrectly estimate transpiration for pixels without vegetation.

The common bean was cultivated under rainfed conditions; however, values of ET found within the rainy season analyzed in this study are the same magnitude of that found under irrigation conditions. Common bean in the Cerrado is also frequently planted in the dry season under pivot irrigation (under full flowering stage). Fietz et al. (2015) obtained values around 4.9 mm day^{-1} for irrigated areas against 4.6 mm day^{-1} in our study. Rodrigues et al. (2013) also recorded higher water demand and evapotranspiration of common bean along the climax of the reproductive period with average values of 4.6 mm day^{-1}. Under no-till, the presence of straw on the soil surface decreases the speed of runoff, prolonging the time available for water infiltration into the soil. The stability of soil structure and the rate of water infiltration into the protected soil are higher under no-tillage compared to an uncovered and desaggregated soil, resulting in a significant reduction in water loss due to runoff (Klein & Libardi, 2000; Stone et al., 2006). Therefore, under no-tillage systems soils can store more water from rain. Obtaining ET values is essential not only to calculate the amount of water required for irrigation management but also to conduct research related to agroclimatic zoning or to monitor soil moisture levels in non-irrigated crops, among other applications (Albuquerque & Coelho, 2021).

In the pasture area, there is a variation within the analyzed plot (Fig. 10), with stretches with a better-preserved pasture, presenting a higher ET. This variation is due to the entry of animals, which occurred on December 9, 2021, precisely on the date after the collection of the image, with a significant reduction in ET in a sequence of decrease until the exhaustion of the area by garrote grazing. The water dynamics in the pasture area is impacted by the presence of animals, since it causes the reduction of biomass, the redistribution of nutrients, and the mechanical impact of trampling, affecting ecological processes (Giese et al., 2019). Analyzing the ET behavior among the three land uses (Fig. 10), the results indicate that forest areas favor the increase of ET, being attributed to this characteristic of the most developed vegetation structure, with high soil cover and deep roots. Land use planning and management are intrinsically linked to the preservation of water resources, since changes in land use have a direct influence on the amount of water available through significant hydrological processes (Guo et al., 2008). It is noteworthy that the hydrological cycle of the Cerrado can be modified

with increased anthropization, from the insertion of pasture (exotic grasses) and agricultural crops.

Conclusions

The UAV-based method to determine evapotranspiration (ET) parameters offers advantages, such as the ability to collect data on cloudy days, complementing satellite data gaps, and achieving centimeter resolution, which makes it easier to identify land uses with significant deviations in water consumption. This resulted in an average spatial resolution gain of 5.8 cm compared to Sentinel-2 satellite data, enabling more specific management of areas of interest. UAV-based data is applicable in certain plant conditions, offering a more specific understanding of the plant's water deficit. This tool allows a detailed analysis of canopy water conditions in different areas, including agricultural crops, pastures, and native vegetation, e.g., forests. Calibrations can be performed using the data obtained via the eddy covariance method (EC) to improve the accuracy of the data obtained by UAV, increasing the assertiveness of the estimates. However, the spatial range of the EC method is limited to a level of a plot. The SAFER model applied in this study used input data from the UAV and weather station, allowing ET to be obtained according to demand, which favors the discussion on ET behavior and variation, highlighting the importance of agricultural practices that promote water storage in plants and soil and minimize negative impacts on the Cerrado landscape. Although it must be mentioned that however UAVs improve soil–plant separation because of their high resolution and the more accurate results, it is a tool for smaller area surveys. To obtain this, resolution with UAVs requires a lot of time and resources. Therefore, the use of UAVs and satellites should be considered complementary, the information obtained by sensors in drones being a powerful tool for refining satellite-born data whenever necessary.

Acknowledgements We appreciate the contribution of Brazil's National Council for Scientific and Technological Innovation (CNPq) and Coordination for the Improvement of Higher Education Personnel (CAPES) in the form of scholarships G.S.A.L (Grant N° 001). M.E.F. and B.E.M. are CNPq research fellows (Grant N° 317013/2023-8 and 307807/2022-3, respectively). We also acknowledge the support by the National Institute of Science and Technology in Low Carbon Emission Agriculture (INCT-ABC) sponsored by Brazil's National Council for Scientific and Technological Development (CNPq, Grant N° 406635/2022-6) and by the Ministry of Agriculture (MAPA).

Author contribution Gabriella Santos Arruda de Lima led the study, conceptualized, designed, and performed the research; Jepherson Correia Sales, Joelson de Souza Passos, Beata Emoke Madari, Manuel Eduardo Ferreira, Márcia Thaís de Melo Carvalho, Pedro Luiz Oliveira de Almeida Machado participated in data curation, writing, reviewing, and editing the draft. Beata Emoke Madari, Manuel Eduardo Ferreira, Márcia Thaís de Melo Carvalho, Pedro Luiz Oliveira de Almeida Machado funding acquisition.

Funding This publication is based upon work supported by the Embrapa "INTEGRA Carbono" project (Grant N° SEG 20.18.03.043) and the "Projeto Rural Sustentavel – Cerrado" in partnership with the Inter-American Development Bank (IDB), the UK Government, the Ministry of Agriculture of Brazil, the Brazilian Institute for Development and Sustainability (IABS), and the ICLF Network Association. The authors acknowledge the financial support through the partners of the Joint Call of the Cofund ERA-Net SusCrop (Grant N° 771134), FACCE ERA-GAS (Grant N° 696356), ICT-AGRI-FOOD (Grant N° 862665) and SusAn (Grant N° 696231) and to ERA-Net Cofund 2021 "SENSE" project (Grant N° 109) as well as funding by the New Zealand Government to support the objectives of the Global Research Alliance on Agricultural Greenhouse Gases (Grant N° 20.22.00.184).

Data availability No datasets were generated or analysed during the current study.

Declarations

Ethics approval All authors have read, understood, and complied as applicable with the statement on "Ethical responsibilities of Authors" as found in the Instructions for Authors.

Consent for publication This paper has not been published elsewhere.

Competing interests The authors declare no competing interests.

References

Albuquerque, P. E. P. de., & Coelho, E. A. (2021). Planilha para obtenção de coeficiente de cultura (Kc) para culturas de ciclo anual, segundo método FAO, para as condições climáticas brasileiras (Comunicado Técnico, 254). Sete Lagoas: Embrapa Milho e Sorgo. http://www.infoteca.cnptia.embrapa.br/infoteca/handle/doc/1136374. Accessed 5 Aug 2023.

Aliabad, F. A., Shojaei, S., Mortaz, M., Ferreira, C. S. S., & Kalantari, Z. (2022). Use of Landsat 8 and UAV images to assess changes in temperature and evapotranspiration by economic trees following foliar spraying with light-reflecting compounds. *Remote Sens, 14*(23), 6153. https://doi.org/10.3390/rs14236153

Allen, R. G., Pereira, L. S., Raes, D., & Smith, M. (1998). Crop evapotranspiration: Guidelines for computing crop water requirements. Rome: FAO. 300 p. (FAO. Irrigation and drainage paper, 56.

Allen, R.G., Hartogensis, O., & de Bruin H.A.R. (2000), Long-wave radiation over alfafa during the RAPID feld campaign in Southern Idaho; *Research report*. Univ of Idaho, Kimberly

Bastiaanssen, W. G. M., Pelgrum, H., Wang, J., Ma, Y., Moreno, J. F., Roerink, G. J., & van der Wal, T. (1998). A remote sensing surface energy balance algorithm for land (SEBAL): Part 2: Validation. *Journal of Hydrology, 212–213*, 213–229. https://doi.org/10.1016/S0022-1694(98)00254-6

Caioni, C., Silvério, D. V., Macedo, M. N., Coe, M. T., & Brando, P. M. (2020). Droughts amplify differences between the energy balance components of Amazon forests and croplands. *Remote Sensing, 12*(3), 525. https://doi.org/10.3390/rs12030525

Chen, Y., Xia, J., Liang, S., Feng, J., Fisher, J. B., Li, X., Li, X., Liu, S., Ma, Z., & Miyata, A. (2014). Comparison of satellite-based evapotranspiration models over terrestrial ecosystems in China. *Remote Sensing of Environment, Elsevier, 140*, 279–293. https://doi.org/10.1016/j.rse.2013.08.045

Cheng, M., Sun, C., Nie, C., Liu, S., Yu, X., Bai, Y., Liu, Y., Meng, L., Jia, X., Liu, Y., Zhou, L., Nan, F., Cui, T., & Jin, X. (2023). Evaluation of UAV-based drought indices for crop water conditions monitoring: A case study of summer maize. *Agricultural Water Management, 287*, 108442. https://doi.org/10.1016/j.agwat.2023.108442

Christofidis, D. (2001). Os recursos hídricos e a prática da irrigação no Brasil e no mundo. *Revista ITEM: Irrigação e Tecnologia*, (49), 8–13. Retrieved June 5, 2023, from https://abid.org.br/Recursos/Arquivos/item_49.pdf

Cihlar, J. (2000). Land cover mapping of large areas from satellites: Status and research priorities. *International Journal of Remote Sensing*, (21), 1093- 1114. https://doi.org/10.1080/014311600210092

Dias, L.C.P., Macedo, M.N., Costa, M.H., Coe, M.T., & Neill, C. (2015). Effects of land cover change on evapotranspiration and streamflow of small catchments in the Upper Xingu River Basin, Central Brazil. *Journal of Hydrology: Regional Studies,* 4(Part B), 108–122. https://doi.org/10.1016/j.ejrh.2015.05.010.

Doorenbos, J., & Pruitt, W. O. (1977). *Crop water requirements* (FAO Irrigation and drainage paper, 24). Rome: FAO. Retrieved from http://www.fao.org/3/a-s8376e.pdf, accessed on July 3, 2023.

Ebert, L. A., Talib, A., Zipper, S. C., Desai, A. R., Paw, U. K. T., Chisholm, A. J., Prater, J., & Nocco, M. A. (2022). How high to fly? Mapping evapotranspiration from remotely piloted aircrafts at different elevations. *Remote Sensing, 14*(7), 1660. https://doi.org/10.3390/rs14071660

Ferreira, M. E., Nogueira, S. H. M., Latrubesse, E. M., Macedo, M. N., Callisto, M., Bezerra Neto, J. F., & Fernandes, G. W. (2022). Dams pose a critical threat to rivers in Brazil Cerrado hotspot. *Water, 14*(22), 3762–3778. https://doi.org/10.3390/w14223762

Fietz, C. R., Comunello, E., Flumignan, D. L., & Ceccon, G. (2015). Evapotranspiração e coeficientes de cultivo do feijão-caupi nas condições climáticas de Mato Grosso do Sul. In XIX Congresso Brasileiro de Agrometeorologia. Lavras, MG, Brazil. Retrieved from https://www.alice.cnptia.embrapa.br/alice/bitstream/doc/1027811/1/C.Agrometeorologiap.144.pdf, accessed on October 24, 2022.

French, A. N., Hunsaker, D. J., & Thorp, K. R. (2015). Remote sensing of environment remote sensing of evapotranspiration over cotton using the TSEB and METRIC energy balance models. *Remote Sensing of Environment., 158*, 281–294. https://doi.org/10.1016/j.rse.2014.11.003

Messina, G.; Peña, J.M.; Vizzari, M.; & Modica, G. (2020). A comparison of UAV and satellites multispectral imagery in monitoring onion crop. An Application in the 'Cipolla Rossa di Tropea' (Italy). *Remote Sensing*, 12(20), 3424. https://doi.org/10.3390/RS12203424

Giese, E., Rockler, A., Shirmohammadi, A., & Pavao-Zuckerman, M. (2019). Assessing watershed-scale stormwater green infrastructure response to climate change in Clarksburg, Maryland. *Journal of Water Resources Planning and Management, 145*(10), 05019015. https://doi.org/10.1061/(ASCE)WR.1943-5452.0001099

R Gregory L Haly Neely., Cristine, L.S., Morgan., & Chenghai, Yang. 2018 Spatial analysis of multispectral and thermal imagery from multiple platforms In Autonomous Air and Ground Sensing Systems for Agricultural Optimization and Phenotyping III 10664 210 220 https://doi.org/10.1117/12.2305896

Guo, H., Hu, Q., & Jiang, T. (2008). Annual and seasonal stream flow responses to climate and land-cover changes in the Poyang Lake basin. *China. Journal of Hydrology, 355*(1–4), 106–122. https://doi.org/10.1016/j.jhydrol.2008.03.020

Hafeez, S., Khan, A. R., Al-Quraan, M., Mohjazi, L., Zoha, A., Imran, M. A., & Sun, Y. (2023). Blockchain-assisted UAV communication systems: A comprehensive survey. *IEEE Open Journal of Vehicular Technology, 4*, 558–580. https://doi.org/10.1109/OJVT.2023.3295208

Hernandez, F. B. T., Teixeira, A. H. C., Neale, C. M. U., & Taghvaeian, S. (2014). Large scale actual evapotranspiration using agro-meteorological and remote sensing data in the northwest of Sao Paulo State, Brazil. *Acta Horticulturae*, 1038(3), 263–270. https://doi.org/10.17660/ActaHortic.2014.1038.31

Hoffman, G. S., Silva, R. C., Weber, E. J., Barbosa, A. A., Oliveira, L. F. B., Alves, R. J. V., Hasenack, H., Schossler, V., Aquino, F. E., & Cardoso, M. F. (2023). Changes in atmospheric circulation and evapotranspiration are reducing rainfall in the Brazilian Cerrado. *Nature Portfolio, 13*, 11236. https://doi.org/10.1038/s41598-023-38174-x

Holman, F. H., Riche, A. B., Castle, M., Wooster, M. J., & Hawkesford, M. J. (2019). Radiometric calibration of 'commercial off the shelf' cameras for UAV-based high-resolution temporal crop phenotyping of reflectance and

NDVI. *Remote Sensing, 11*(14), 1657. https://doi.org/10.3390/RS11141657

Ivo, I. O., Biudes, M. S., Vourlite, G. L., Machado, N. G., & Martim, C. C. (2020). Effect of fires on biophysical parameters, energy balance and evapotranspiration in a protected area in the Brazilian Cerrado. *Remote Sensing Applications: Society and Environment., 19*, 100342. https://doi.org/10.1016/j.rsase.2020.100342

Kalnay, E., Kanamitsu, M., Kistler, R., Collins, W., Deaven, D., Gandin, L., & Zhu, Y. (1996). The NCEP/NCAR 40-year reanalysis project. *Bulletin of the American Meteorological Society, 77*(3), 437–471. https://doi.org/10.1175/1520-0477(1996)077/3C0437:TNYRP/3E2.0.CO;2

Klein, V. A., & Libardi, P. L. (2000). Faixa de umidade menos limitante ao crescimento vegetal e sua relação com a densidade do solo ao longo do perfil de um latossolo roxo. *Ciência Rural, 30*(6), 959–964. https://doi.org/10.1590/s0103-84782000000600006

Kljun, N., Calanca, P., Rotach, M. W., & Schmid, H. P. (2015). A simple two-dimensional parameterisation for Flux Footprint Prediction (FFP). *Geoscientific Model Development, 8*(11), 3695–3713. https://doi.org/10.5194/gmd-8-3695-2015

Lu, S., Xuan, J., Zhang, T., Bai, X., Tian, F., & Ortega-Farias, S. (2022). Effect of the shadow pixels on evapotranspiration inversion of vineyard: A high-resolution UAV-based and ground-based remote sensing measurements. *Remote Sensing, 14*(9), 2259. https://doi.org/10.3390/rs14092259

Maitiniyazi, M., Vasit, S., Paheding, S., Ahmad, M., Daloye, E., Erkbol, H., & Fritschi, F. B. (2020). Crop monitoring using satellite/UAV data fusion and machine learning. *Remote Sensing, 12*(9), 1357. https://doi.org/10.3390/RS12091357

MAPBIOMAS. (2022). *Destaques do mapeamento anual de cobertura e uso da terra entre 1985 a 2021: Cerrado.* Available at https://brasil.mapbiomas.org/soja-ocupa-10-do-cerrado. Retrieved on January 15, 2024.

Ministério do Meio Ambiente e dos Recursos Naturais Renováveis (MMA). (2014). *Ppcerrado—Plano de Ação para Prevenção e Controle do Desmatamento e das Queimadas no Cerrado: 2ª Fase (2014–2015).* Brasília, DF, Brazil: Instituto do Meio Ambiente e dos Recursos Naturais Renováveis. 132p. Retrieved from https://documentacao.socioambiental.org/noticias/anexo_noticia/10046_20100317_144341.pdf on February 4, 2023.

Mokhtari, A., Ahmadi, A., Daccache, A., & Dreschsler, K. (2021). Actual evapotranspiration from UAV images: A multi-sensor data fusion approach. *Remote Sensing., 13*(12), 2315. https://doi.org/10.3390/rs13122315

Nassar, A., Torres-Rua, A., Kustas, W., Nieto, H., McKee, M., Hipps, L., Stevens, D., Alfieri, J., Prueger, J., Alsina, M. M., et al. (2020). Influence of model grid size on the estimation of surface fluxes using the two source energy balance model and sUAS imagery in vineyards. *Remote Sensing., 12*(3), 342. https://doi.org/10.3390/rs12030342

Oliveira, R. S., Bezerra, L., Davidson, E. A., Pinto, F., Klink, C. A., Nepstad, D. C., & Moreira, A. (2005). Deep root function in soil water dynamics in Cerrado Savannas of Central Brazil. *Functinal Ecology., 19*, 574–581. https://doi.org/10.1111/j.1365-2435.2005.01003.x

Paul, G., Gowda, P. H., Vara Prasad, P. V., Howell, T. A., Aiken, R. M., & Neale, C. M. U. (2014). Investigating the influence of roughness length for heat transport (Zoh) on the performance of SEBAL in semi-arid irrigated and dryland agricultural systems. *Journal of Hydrology, 509*, 231–244. https://doi.org/10.1016/j.jhydrol.2013.11.040

Pan, S., Liu, L., Bai, Z., & Xu, Y. P. (2018). Integration of remote sensing evapotranspiration into multiobjective calibration of distributed hydrology–soil–vegetation model (DHSVM) in a humid region of China. *Water, 10*(12), 1841. https://doi.org/10.3390/w10121841

PIX4Dmapper, Version 4.4.12. Professional photogrammetry software for drone mapping. (2022). Available online: https://www.pix4d.com/product/pix4dmapper-photogrammetry-software (accessed on 27 October 2022).

de Queiroz, F. A. (2009). Impactos da sojicultura de exportação sobre a biodiversidade do Cerrado. *Sociedade & Natureza, 21*(2), 193–209. https://doi.org/10.1590/S1982-45132009000200013

Rodrigues, A. C., Bonifacio, A., Antunes, J. E. L., Silveira, J. A. G., & Figueiredo, M. V. B. (2013). Minimization of oxidative stress in cowpea nodules by the interrelation ship between *Bradyrhizobium sp*. and plant growth-promoting bacteria. *Applied Soil Ecology, 64*, 245–251. https://doi.org/10.1016/j.apsoil.2012.12.018

Ruhoff, A. L., Paz, A. R., Collischonn, W., Aragao, L. E. O. C., Rocha, H. R., & Malhi, Y. S. (2012). A modis-based energy balance to estimate evapotranspiration for clear-sky days in Brazilian Tropical Savannas. *Remote Sensing, 4*(3), 703–725. https://doi.org/10.3390/rs4030703

Safre, A. L. S., Nassar, A., Torres-Rua, A., et al. (2022). Performance of Sentinel-2 SAFER ET model for daily and seasonal estimation of grapevine water consumption. *Irrigation Science, 40*, 635–654. https://doi.org/10.1007/s00271-022-00810-1

Sales, D. L. A., Alves Júnior, J., Souza, J. M. F., Casaroli, D., Evangelista, A. W. P., & Pereira, R. M. (2016). Common bean evapotranspiration estimated by orbital images. *African Journal of Agricultural Research, 11*(10), 867–872. https://doi.org/10.5897/AJAR2015.10500

Sano, E.E., Rosa, R., Scaramuzza, C.A.D.M., Adami, M., Bolfe, E.L., Coutinho, A.C., Esquerdo, J.C.D.M., Maurano, L.E.P., Narvaes, I.D.S., De Oliveira Filho, F.J.B., et al. (2019). Land use dynamics in the Brazilian Cerrado in the period from 2002 to 2013. *Pesquisa Agropecuária Brasileira*, 54. https://doi.org/10.1590/S1678-3921.pab2019.v54.00138

Santesteban, L. G., Di Gennaro, S. F., Herrero-Langreo, A., Miranda, C., Royo, J. B., & Matese, A. (2017). High-resolution UAV-based thermal imaging to estimate the instantaneous and seasonal variability of plant water status within a vineyard. *Agricultural Water Management, 183*, 49–59. https://doi.org/10.1016/j.agwat.2016.08.026

Santos, C. V. B., Moura, M. S. B., Galvíncio, J. D., Carvalho, H. F. S., Miranda, R. Q., & Montenegro, S. M. G. L. (2021). Comparação de imagens multiespectrais utilizando Satélites e VANT para a análise de mudanças estruturais em área de Floresta Seca. *Revista Brasileira de Geografia Física*, 14, 2510–2522. https://doi.org/10.26848/rbgf.v14.5.p2510-2522

Silva Oliveira, B., Moraes, C. E., Carrasco-Benavides, M., Bertani, G., & Mataveli, G. A. V. (2018). Improved albedo estimates implemented in the METRIC model for modeling energy balance fluxes and evapotranspiration over agricultural and natural areas in the Brazilian Cerrado. *Remote Sensing, 10*(8), 1181. https://doi.org/10.3390/rs10081181

Silva, H. J. F., Gonçalves, W. A., & Bezerra, B. G. (2019). Comparative analyses and use of evapotranspiration obtained through remote sensing to identify deforested areas in the Amazon. *International Journal of Applied Earth Observation and Geoinformation, 78*, 163–174. https://doi.org/10.1016/j.jag.2019.01.015

Stone, L. F., Da Silveira, P. M., Moreira, J. A. A., & Braz, A. J. B. P. (2006). Evapotranspiração do feijoeiro irrigado em plantio direto sobre diferentes palhadas de culturas de cobertura. *Pesquisa Agropecuária Brasileira, 41*(4), 577–582. https://doi.org/10.1590/S0100-204X2006000400005

Strassburg, B. B. N., Brooks, T., Feltran-Barbieri, R., Iribarrem, A., Crouzeilles, R., Loyola, R., Latawiec, A. E., Oliveira Filho, F. J. B., Scaramuzza, C. A. M., Scarano, F. R., Soares-Filho, B., & Balmford, A. (2017). Moment of truth for the Cerrado hotspot. *Nature Ecology & Evolution, 1*(4), 0099. https://doi.org/10.1038/s41559-017-0099

Sumanta, Das., Christopher, J., Apan, A., Choudhury, M.R., Chapman, S., Menzies, N.W., Yash, P., & Dang, Y. P., (2020). UAV-thermal imaging: A robust technology to evaluate in-field crop water stress and yield variation of wheat genotypes. 138–141. https://doi.org/10.1109/InGARSS48198.2020.9358955

Teixeira, A. H. C., & Lima Filho, J. M. P. Clima. In: MOUCO, M. A. C. (Ed.). (2004). Cultivo da mangueira. Petrolina: Embrapa SemiÁrido. (Sistema de Produção). http://www.infoteca.cnptia.embrapa.br/infoteca/handle/doc/884451. Accessed 5 May 2023.

Teixeira, A. H. C., Bastiaanssen, W. G. M., Ahmad, M. D., Bos, M. G., & Moura, M. S. B. (2008). Analysis of energy fuxes and vegetation-atmosphere parameters in irrigated and natural ecosystems of semi-arid Brazil. *Journal of Hydrology, 362*, 110–127. https://doi.org/10.1016/j.jhydrol.2008.08.011

Teixeira, A. H. C. (2010). Determining regional actual evapotranspiration of irrigated and natural vegetation in the São Francisco river basin (Brazil) using remote sensing an Penman-Monteith equation. *Remote Sensing, 2*(5), 1287–1319. https://doi.org/10.3390/rs0251287

Teixeira, A. H. C., Hernandez, F. B. T., & Lopes, H. L. (2012). Application of Landsat images for quantifying the energy balance under conditions of fast land use changes in the semi-arid region of Brazil. In *SPIE Remote Sensing 2012, Edinburgh*. Proceedings. Edinburgh: SPIE. https://doi.org/10.1117/12.965882

Teixeira, A. H. C., Scherer-Warren, M., Hernandez, F. B. T., Andrade, R. G., & Leivas, J. F. (2013). Large-scale water productivity assessments with MODIS images in a changing semi-arid environment: A Brazilian case study. *Remote Sensing., 5*(11), 5783–5804. https://doi.org/10.3390/rs5115783

Teixeira, A.H.C., Victoria D.C., Andrade R.G., Leivas, J.F., Bolfe, E.L., & Cruz, C.R. (2014a). Coupling of MODIS images and agrometeorological data for agricultural water productivity analyses in the Mato Grosso State, Brazil. In: *Proceedings of SPIE*, (9239), 92390W-1–92390W-14. https://doi.org/10.1117/12.2065967

AHC Teixeira FBT Hernandez HL Lopes M Scherer-Warren LH Bassoi 2014b A comparative study of techniques for modeling the spatiotemporal distribution of heat and moisture fluxes in different agroecosystems in Brazil GG Petropoulos Eds Remote sensing of energy fuxes and soil moisture content, 1edn Florida 169 191

Teixeira, A. H. C., Padovani, C. R., Andrade, R. G., Leivas, J. F., Victoria, D. D. C., & Galdino, S. (2015). Use of MODIS images to quantify the radiation and energy balances in the Brazilian Pantanal. *Remote Sensing, 7*(11), 14597–14619. https://doi.org/10.3390/rs71114597

Sagan, V., Maimaitijiang, M., Sidike, P., Maimaitiyiming, M., Erkbol, H., Hartling, S., Peterson, K., Peterson, J., Burken, J. G., & Fritschi, F. (2019). UAV/satellite multiscale data fusion for crop monitoring and early stress detection. ISPRS - International Archives of the Photogrammetry, Remote Sensing and Spatial Information Sciences. https://doi.org/10.5194/isprs-archives-XLII-2-W13-715-2019

Sampaio, G., Nobre, C., Costa, M. H., Satyamurty, P., Soares-Filho, B. S., & Cardoso, M. (2007). Regional climate change over eastern Amazonia caused by pasture and soybean cropland expansion. *Geophysical Research Letters, 34*, L17709. https://doi.org/10.1029/2007GL030612

Veloso, G. A., Ferreira, M. E., & Silva, B. B. (2017). Determinação da evapotranspiração real diária em áreas irrigadas do Projeto Jaíba (Minas Gerais, Brasil), mediante imagens Landsat 5 - TM. *Revista Cerrados*, 15(1), 53–76. https://doi.org/10.22238/rc24482692v15n12017p53a76

Xia, T., Kustas, W. P., Anderson, M. C., Alfieri, J. G., Gao, F., McKee, L., Prueger, J. H., Geli, H. M. E., Neale, C. M. U., Sanchez, L., Alsina, M. M., & Wang, Z. (2016). Mapping evapotranspiration with high-resolution aircraft imagery over vineyards using one- and two-source modeling schemes. *Hydrology and Earth System Sciences, 20*(4), 1523–1545. https://doi.org/10.5194/hess-20-1523-2016

Ye, L., Zahra, M. M. A., Albedyry, N. K., & Yaseen, Z. M. (2022). Daily scale evapotranspiration prediction over the coastal region of southwest Bangladesh: New development of artificial intelligence model. *Stochastic Environmental Research and Risk Assessment, 36*(2), 451–471. https://doi.org/10.1007/s00477021020554

Zamani-Noor, N., & Feistkorn, D. (2022). Monitoring growth status of winter oilseed rape by NDVI and NDYI derived from UAV-based red–green–blue imagery. *Agronomy*, 12(9), 2212. https://www.mdpi.com/2073-4395/12/9/2212#